

Article

The Thermophysical Aspects of the Transformation of Porous Structures in Versatile Nanostructured Materials

Hanna Koshlak ^{1,*} , Borys Basok ² , Anatoliy Pavlenko ¹ , Tatiana Hrabova ² and Vitalii Opryshko ^{2,3}

¹ Department of Sanitary Engineering, Kielce University of Technology, Aleja Tysiąclecia Państwa Polskiego, 7, 25-314 Kielce, Poland; apavlenko@tu.kielce.pl

² Institute of Engineering Thermophysics of the National Academy of Sciences of Ukraine, Marii Kapnist, 2a, 03057 Kyiv, Ukraine; borys.basok@gmail.com (B.B.); gtl@ukr.net (T.H.); opryshko@ill.kpi.ua (V.O.)

³ National Technical University of Ukraine “Igor Sikorsky Kyiv Polytechnic Institute”, 03056 Kyiv, Ukraine

* Correspondence: hkoshlak@tu.kielce.pl

Abstract: The technology of obtaining porous nanostructures is based on ecological organosilicon materials and their uses in some spheres of human life, for example, for medical preparations, for thermal insulation of building structures and industrial equipment, and for cleaning. The purpose of this study was to establish correlations between various experimental parameters (shear stress, speed pulsations, temperature, viscosity, and processing time) and the rheological characteristics of suspensions obtained by the method of liquid-phase dispersion; it was a study of hydrodynamic effects and the processes of heat and mass exchange in liquid systems during the liquid-phase dispersion of hydrogel monoliths by means of discrete-pulse activation in a special rotary apparatus. The dehydration of hydrogels was carried out by two methods: convective drying in a layer and spraying in the coolant flow. Experiments have shown that the key parameters for obtaining stable homogeneous suspensions are a synergistic combination of concentration factors and processing time. To obtain adsorbents in the form of pastes with specified adsorption properties and a monolith size of up to 300 μm , the optimal parameters were a hydrogel concentration of 70% and a processing time in the double-recirculation mode. Xerogels obtained by convective drying are a polydisperse mixture of strong monoliths and fragile aggregates. In contrast, xerogel monoliths obtained by spray drying show great homogeneity in terms of dispersion and strength characteristics. The rheological parameters of the hydrogel dispersions, which depend on the concentration and hydrodynamic treatment modes, are the dominant factors affecting the moisture extraction during drying. This study marks the first investigation into the resilience of porous organosilicon structures against the influence of intense turbulence fields and mechanical stresses experienced within the rotor apparatus during suspension production.

Keywords: eco-friendly organosilicon materials; xerogel; aerogel; rotary dispersion technology; homogeneous suspension; rheological behavior; drying; sustainable nanostructure materials



Citation: Koshlak, H.; Basok, B.; Pavlenko, A.; Hrabova, T.; Opryshko, V. The Thermophysical Aspects of the Transformation of Porous Structures in Versatile Nanostructured Materials. *Sustainability* **2024**, *16*, 2673. <https://doi.org/10.3390/su16072673>

Academic Editors: Lokendra Pal, Preeti Tyagi and Lucian Lucia

Received: 13 February 2024

Revised: 14 March 2024

Accepted: 15 March 2024

Published: 25 March 2024



Copyright: © 2024 by the authors. Licensee MDPI, Basel, Switzerland. This article is an open access article distributed under the terms and conditions of the Creative Commons Attribution (CC BY) license (<https://creativecommons.org/licenses/by/4.0/>).

1. Introduction

Porous structures find broad practical utility across various domains, serving as versatile materials for insulation, energy conservation, carrier matrices for drug substances, sorbents, catalysts, filters, membranes, sensors, heat insulating materials, and more [1–3].

The most recent comprehensive evaluations of research progress in this field are presented in a series of reviews [4–12], which encompass a diverse array of final applications, such as those in electronics [13,14], alongside thorough theoretical analyses [15,16]. Several of these reviews underscore the importance of environmental restoration through sustainable development [5], heightened focus on industrial ecology [11,12], and advancements aimed at enhancing living standards and human health [6,8,10].

The applicability of these structures is determined by the physical and chemical attributes of their surfaces and their inherent porosity. The qualitative features of porous

materials hinge upon factors such as pore shape and size, quantitative proportions, connectivity, spatial distribution, and the nuances of porous structure formation, which, in turn, are contingent upon the chosen production method aligned with the material's functional objectives [17–21]. For instance, the characteristics of catalysts or adsorbents structures, including porosity and the nature of active sites on the material's surface, exert a pivotal influence on catalytic or adsorptive activities. Alterations in porosity can bring about changes in reaction rates and the functional efficiency of materials, influencing heat and mass transfer and reagent and product diffusion, among other factors [22,23]. When the volume of pores equals or exceeds the volume of the substance constituting the material's structure, the designation of nanoporous material is invoked. Depending on the manner in which the pore space is configured, these structures are categorized as spatial frameworks formed by spherical particles, cellular structures, monoliths with channels, or laminates [18]. In terms of pore size, structures are further classified into microporous (pore size < 2 nm), mesoporous (pore size 2–50 nm), and macroporous (pore size > 50 nm) [24].

The prevalent techniques for synthesizing hierarchically organized porous structures, such as hydrogels, xerogels, and aerogels, predominantly involve sol-gel technologies. The sol-gel synthesis process is multifaceted, encompassing stages like a precursor solution preparation, structure and pore space formation, ripening and syneresis, washing, drying, and heat treatment to yield xerogels in powder form. The structuring of powders into macroscopic porous monoliths is achieved through extrusion, granulation, gel-casting, matrix-coating, convective-drying, and dry-pressing methodologies [25–29]. For the production of suspensions containing porous particles, an intermediate state in the creation of monolithic structures, liquid-phase dispersion and homogenization are employed. These processes can be executed under conditions of high shear stresses, employing cavitation effects, in bead or vibration mills [30–34]. The practical applicability of suspensions is determined by their rheological properties, which need to be optimized for specific processes of nanostructure formation [35]. In injection molding technologies, for instance, highly concentrated suspensions with high plasticity and a yield point are utilized, whereas slip casting typically employs Newtonian suspensions (diluted) [1]. The structural and mechanical properties of suspensions during dehydration by spraying influence the morphology and dispersion characteristics of resulting dry powders [27,36,37].

The rheological behavior of suspensions is determined by the forces of interaction between particles and their size within the dispersed system. Repulsive forces yield a homogeneous dispersed suspension, while attractive forces can result in an agglomerated, viscous suspension exhibiting significant yield strength [31,32].

Critical to the formation of porous gel structures are the processes associated with liquid removal, which occupies the space between particles and the structural elements of the matrix framework. During dehydration in an air stream or vacuum, substantial internal stresses are generated in the matrix framework of the gel. The removal of the liquid phase leads to significant structural shrinkage, and porosity decreases due to surface tension forces acting during the liquid-removal process. The degree of gel compaction is contingent upon the balance between compression induced by surface tension and the elasticity of the gel framework resisting compression [19,38–40]. The drying process induces considerable stresses in the material, resulting in the occurrence of cracks and the destruction of monolithic samples.

A comparative evaluation of two prevalent drying methods for hierarchically organized porous monoliths synthesized through sol-gel technology has elucidated that evaporation drying exhibits comparable effectiveness to conventional supercritical drying in terms of the material's structural and textural properties, including specific surface area and pore volume. The modulation of pore-space characteristics can be, to a certain extent, accomplished by optimizing temperature and speed modes during the drying process [37,41].

Research into the influence of various factors on the formation of the globular structure of gels has provided the physicochemical foundation for the targeted regulation of the struc-

ture of organic–inorganic adsorbents, specifically hydrogels of polymethylsiloxanes [38]. Consequently, an industrial sol-gel synthesis technology has been developed for Methylsilicic Acid Hydrogel (HGMSA). This biocorrective sorbent demonstrates the capability to efficiently bind and expeditiously remove medium-molecular toxic substances of both endogenous and exogenous origin, along with pathogenic microorganisms and viruses from the human body. This effectiveness stems from its high affinity to adhere to the organic silicon matrix. The adhesion to the sorbent leads to the destruction of bacteria, a process that can be augmented by the presence of metal ions in the adsorbent composition [42,43].

From the preceding discussion, it can be inferred that the utilization of porous silicon-organic sorbents and their derivatives, encompassing enteric, topical, hemosorbents, and parenteral preparations, has facilitated the development of a diverse array of sorption materials tailored for various medical applications. These materials offer significant advantages, including complete harmlessness, non-toxicity, high biocompatibility with human tissues, blood, and other biological substrates, the selective sorption of medium-molecular-weight toxic metabolites, and high adsorption capacity. This domain aligns closely with the principles of sustainable development, particularly in the context of enhancing human health and well-being. Such advancements are especially pertinent in the current scenario of ongoing hostilities in Ukraine, wherein numerous civilians and military personnel necessitate urgent medical attention.

Furthermore, a scientific and technical inference drawn from the analysis of research indicates that the attainment of high-quality porous nanostructured materials necessitates establishing a correlation between physicochemical parameters influencing synthesis and a spectrum of requisite structural, mechanical, and functional properties. However, this linkage remains inadequately understood for the majority of materials.

In this study, we investigate the influence of various physical, chemical, and technological parameters on characteristic effects and processes such as grinding, homogenization, and the drying of substances for the creation of promising porous nanostructured materials (suspensions and xerogels) based on silica, specifically its globule $(\text{RSiO}_{1.5})_n$. A transformation in nanostructures is carried out through local (and discrete) pulsed energy inputs, facilitated by high flow turbulence, significant shear stresses at the liquid–dispersed particle interface, and the destructive effect of alternating the pressure drop within a specially designed rotary-type unit. Subsequent drying is achieved either by blowing through a layer of heated air or by spray drying the flow within the dryer cyclone. The physicochemical properties of the resulting products and their experimental application in specific technological processes are comprehensively investigated in a dedicated laboratory setting.

2. Research Materials and Methods

HGMSA and HGMSA, whose surfaces are modified with complexes of metal ions (Cu^{2+} /Zn-HGMSA), are used as a model structure [44,45]. HGMSA samples were provided by JSC “Ecologoprotective Firm “KREOMA–PHARM” (Kyiv, Ukraine).

2.1. Methods and Equipment

Xerogel samples were prepared through a two-stage process: I—the formulation of a uniform dispersion of hydrogel monoliths HGMSA in purified water; II—the desiccation of the suspensions through convective drying.

Hydrodynamic processing, the purpose of which was to obtain a homogeneous suspension “HGMSA- H_2O ” with a maximum size of monolithic particles of 300 μm , was carried out in the recirculation mode at the experimental setup (Figure 1) [46]. The circulation loop for suspension comprises reactor R1 equipped with an anchor stirrer (AS), where initial system components are introduced. Pump P1 provides suspension transportation to the original flow type rotary-pulsation apparatus (RPA) [47,48], and for recycling, the suspension is redirected back to R1. Throughout the investigation, P1 regulates the flow rate, the circulation duration is monitored, and suspension temperature is measured before/after the RPA and in the reactor.

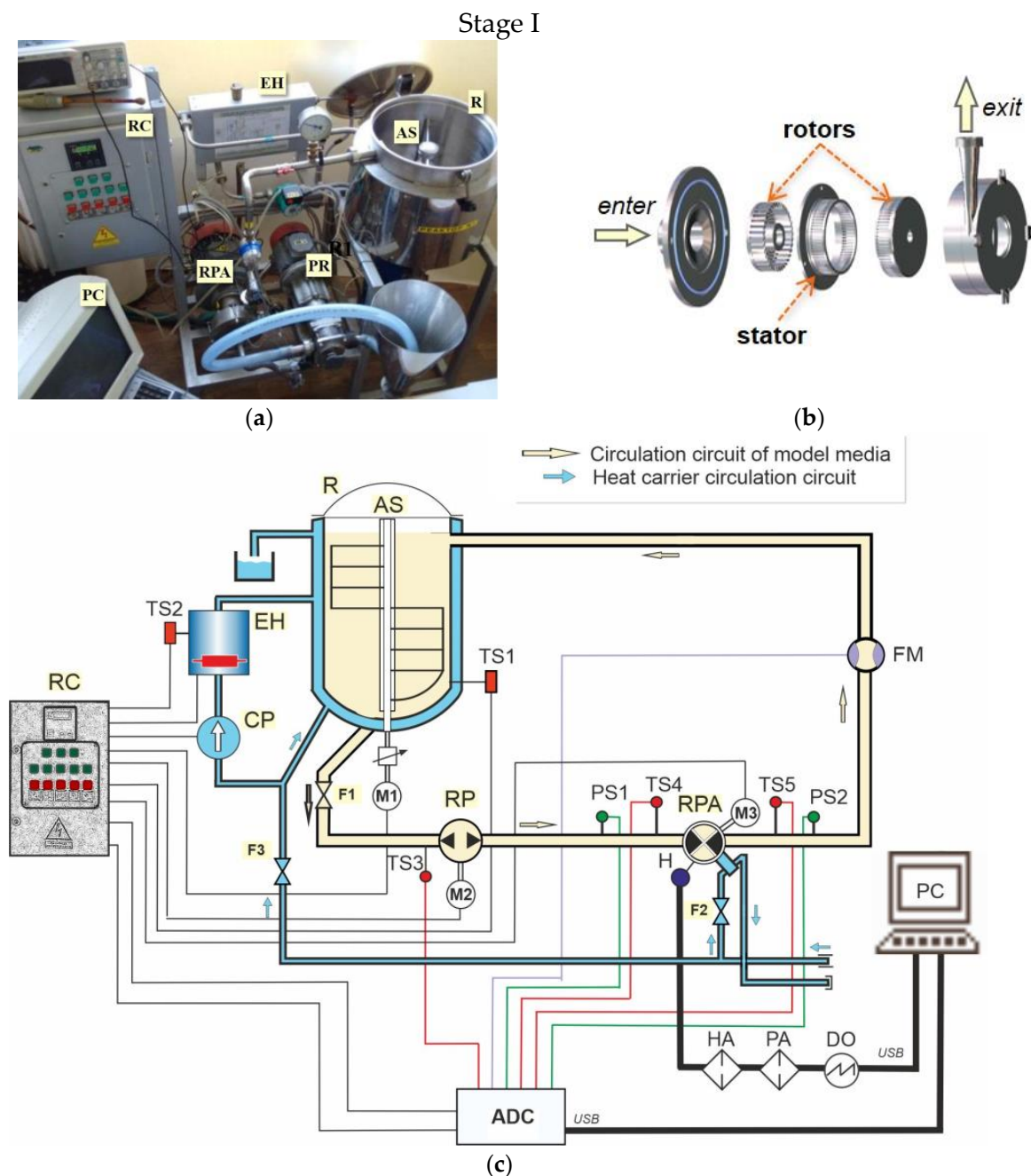


Figure 1. Experimental setup for investigating hydrodynamic effects and heat and mass transfer in fluid systems: visual representation (a); structural components of the rotary-pulsation apparatus (RPA*) (b); schematic diagram of the experimental setup (c). Circulation loop of model media: AS*—anchor stirrer; F1—shut-off and regulating fitting; R*—reactor; RP—rotary pump; RPA*—rotary-pulsation apparatus. Heat carrier circulation loop: CP—centrifugal pump; EH—electric heater; F2, F3—shut-off and regulating fitting. Control and measuring unit: ADS—analogue-to-digital converter; DO—digital oscilloscope; FM—flow meter; H—hydrophone; HA—hydrophone amplifier; P1, P2—pressure sensor; PC—personal computer; PA—preamplifier; RC—remote control; TS1–TS5—temperature sensor. Original designs that were developed and created in Institute of Engineering Thermophysics of the National Academy of Sciences of Ukraine.

The RPA subjects the suspension components to multifactorial influences, employing the discrete-pulse energy-input (DPIE) method for heterogeneous media [30,49–51]. The dispersion of HGMSA monoliths in water is conducted in an apparatus featuring a

rotor–stator–rotor system of working elements. The stator–rotor space of the apparatus generates a maximum shear field at a shear rate of $150,000\text{ s}^{-1}$, perturbed by high-frequency hydrodynamic flow pulsations (1.2–3.6 kHz). Detailed descriptions of design features and geometric dimensions are provided in [48].

The test was iterated a minimum of three times for each experimental series. Data sampling and a selection of samples for subsequent processing and property analysis were based on the adsorption activity of suspensions using Congo red dye. The baseline values for the initial hydrogel and “HGMSA-H₂O” suspensions at ratios of 7:3, 6:4, and 4:6 were 3.3, 2.9, 2.1, and 1.7 mg/g, respectively, with a deviation of $\pm 0.2\text{ mg/g}$.

Convective drying in the layer (layer thickness 30 mm) was carried out by blowing the HGMSA layer with a drying agent (air) with $T_{da} = 120\text{--}150\text{ }^{\circ}\text{C}$ to the final moisture content of the xerogel $W_f = 1.5\text{--}2.0\%$ (Figure 2a). The spray drying was carried out on an experimental RC-1.3 spray dryer with a capacity of 10 kg/h in terms of evaporated moisture equipped with a centrifugal disc sprayer with a rotation speed of 18,000 rpm (Figure 2b) [52].

Stage II

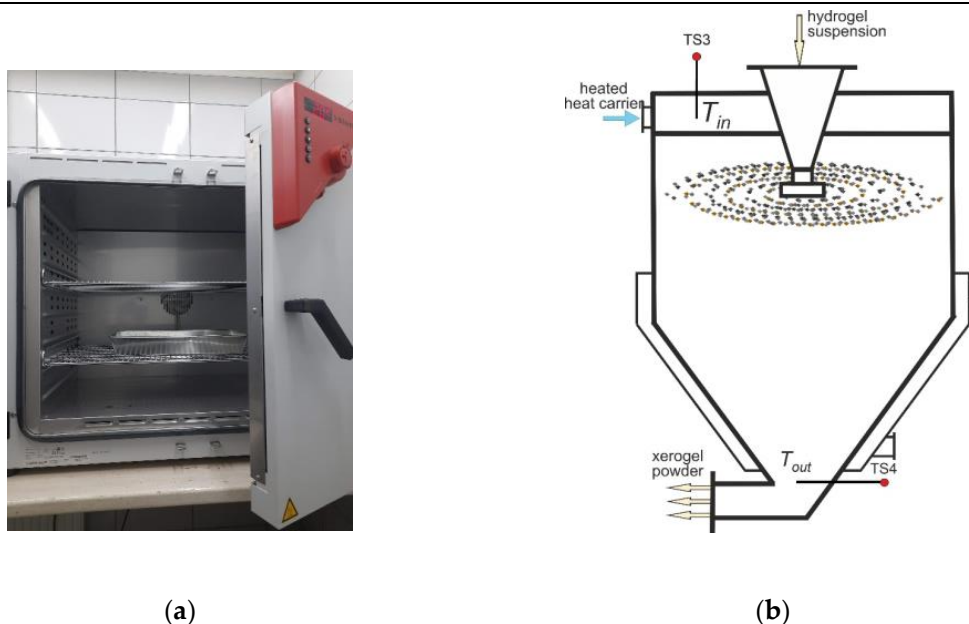


Figure 2. Dehydration of suspensions by convective drying in layer (a) and spray drying (b): TS3–TS4—temperature sensor.

2.2. Research Methods

The adsorption activity of the suspensions was determined in a specialized laboratory of JSC “Ecologoprotective Firm “KREOMA-PHARM” (Ukraine) as the ability to adsorb Congo red dye from an aqueous solution at a concentration of 1.0 mmol/L. The analysis methodology was performed according to [44].

The moisture content of the gels was determined by the arbitrarily drying method at a temperature of $100\text{--}115\text{ }^{\circ}\text{C}$ to a constant mass.

The dispersion analysis of gel samples was evaluated by the morphometric method according to the maximum linear size of monoliths and aggregates using a Mikmed-1 microscope (RF) with a photofixation digital microscope camera eTREK 220x and by the sieve-analysis method using the Vibratory Sieve Shaker ANALYSETTE[®] type 03.502 (FRITSCH GmbH, Idar-Oberstein, Germany) with a set of wire metal sieves followed by measuring the weight on ViBRA[®] AJ (Shinko Denshi Co., Ltd., Tokyo, Japan).

The morphology of the xerogel surfaces was studied on a JSM-9490LV scanning electron microscope (JEOL Ltd., Akishima, Japan) with a magnification factor of $\times 1000$ to $\times 14,000$ and an accelerating voltage of 20 kV.

The structural and sorption characteristics of the xerogels were evaluated by the nonspecific adsorption–desorption of n-hexane on a NovaWin2 complex analyzer (Quantachrome Instrument Corp., Boynton Beach, FL, USA). The algorithms to calculate the specific surface area using the Brunauer–Emmett–Teller method and the size distribution of the sorption pore volume using the Barrett–Joyner–Halenda method are included in the instrument software.

The rheological behavior of the “HGMSA-H₂O” system was studied on a rotational viscometer of type “Rheotest[®] RN” (Rheotest Medingen GmbH, Medingen, Germany) with a rotor/cup H1/G1 measuring pair in continuous deformation mode with a gradual increase in shear rate in the range of 7–1073 s^{−1} at $\dot{\gamma} = 1073$ s^{−1}, while the system was under load for 720 s and, subsequently, at a gradual decrease in the shear rate. The exposure time was 1 min. The study was conducted without a thermostat at a temperature of 18–23 °C.

Each sample underwent a minimum of three measurements. The average mathematical values, derived from these measurements, served as the foundation for constructing graphical dependencies. Experimental data underwent mathematical and statistical analysis using MS Excel and Origin software packages.

3. Results and Discussion

The initial system (HGMSA) is a multiscale “structure with internal structure” type, and at the macro level are wet monoliths and aggregated particles up to 20 mm in size. The structural frame of the monolith consists of a spatial grid of “cross-linked” macromolecules (globules) 7–15 nm in size, in the pores of which there is immobilized water (Figure 3). HGMSA, despite its high humidity (89–91%), lacks fluidity and exhibits plastic and elastic properties [44,45].

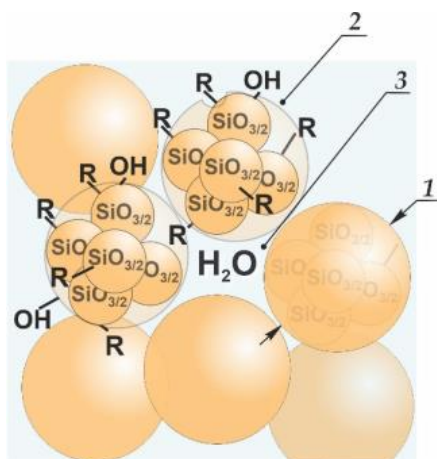


Figure 3. Scheme of the model structure $\{(RSiO_{1.5}) \times nH_2O\}_\infty$: 1—globule; 2—hydration shell; 3—pore with immobilized liquid; (R is an organic radical, n is the number of water molecules).

Organic radicals are placed on the surface of the globule, resulting in hydrophobic (up to 75%) hydrogels and, as a result of uncondensed hydroxyl groups, it is hydrophilic (up to 25%). In the dispersion medium, a hydrate shell (up to four layers of water molecules) is formed on the surface of the globules as a result of electrostatic forces and hydrophilic binding with liquid molecules, which increases the elastic properties of monolithic dispersed particles.

The “HGMSA-H₂O” suspension is characterized by a mixed condensation–coagulation type of structure. On the one hand, HGMSA monoliths have a condensation structure, and coagulation contacts are also formed in water.

Summarizing the above, the studied system is nanostructured and has three types of interaction between dispersed HGMSA particles (atomic, coagulation, and phase).

The development of new structured porous materials and methods for their preparation requires a search for a compromise between certain parameters that determine their functional efficiency. For the system under study, such parameters can be the dispersity of the monoliths, the specific surface area, the size of the pores, and the size of the volume of the adsorption space. The adsorption capacity of the gel, as the main functional indicator of the effectiveness of sorbents, significantly depends on the size of its specific surface, which is determined by the size of globules and the dispersion of the monoliths. In addition, the adsorption pore volume and pore sizes determine such characteristics as the packing density of globules and monoliths.

3.1. Effect of Concentration on the Structural–Adsorption Characteristics of Nanostructures

During hydrodynamic DPIE treatment, the suspension is subjected to a multifactorial effect. Which of the complexes of factors will be dominant depends on the flow regimes determined by the rheological behavior of the suspensions and the concentration of the dispersed phase in the suspension [30,46,49].

The manipulation of hydrogel content in the suspension (refer to Table 1) was undertaken to reduce water content while maintaining sufficient fluidity.

Table 1. The effect of DPIE treatment on structural and adsorption characteristics.

Mass Concentration of HGMSA in H ₂ O	Specific Processing Time	Average Speed of the Temperature Increase in the Suspension	Preferable Final Size of Monolithic and Aggregated Particles (Maximum)	Structural–Adsorption Indicators			
				Specific Surface Area	Sorption Pore Volume	Effective Pore Size Range	Effective Pore Radius
$C_m, \%$	$\tau_{sp}, \text{min/kg}$	$^{\circ}\text{C}/(\text{kg} \times \text{min})$	$\delta^H(\delta_{max}^H), \mu\text{m}$	$S_{sp}, \text{m}^2/\text{g}$	$V_s, \text{cm}^3/\text{g}$	d_{ef}, nm	$\frac{1}{r_{efmax}}, \text{nm}$
100 (original sample)	-	-	-	310	0.890	1.0–13.8	4.56
70	0.08	0.06	65–250 (300)	210	1.623	3.0–27.6	4.61
	0.29	0.10	30–170 (250)	81.3	1.084	3.2–40.0	7.13
60	1.27	0.07	40–70 (120)	60.6	1.064	1.2–20.0	2.77/5.39
	1.39	0.18	30–60 (100)	27	1.012	2.0–30.2	7.4
40	1.8	0.04	20–70 (98)	57.8	1.774	0.4–24.0	3.01/5.37
	3.1	2.67	20–50 (85)	9.8	1.062	1.0–28.8	6.6

This approach aimed to establish optimal conditions for achieving a homogeneous suspension within the recirculation circuit and in the spray-dryer plume.

During the DPIE treatment, the fluid system undergoes a transition from a free-dispersed state to a structured configuration. This process entails the disruption of bonds between aggregated particles within monoliths, the comminution of hydrogel monoliths, the development of hydrate shells around them, and the establishment of novel contact interactions between the newly formed monoliths and their spatial framework. The relative rates of each process component dictate the duration and extent of suspension structuring, with the hydrogel concentration influencing the strength of the framework.

The outcomes of experimental investigations are presented in the form of histograms (Figure 4), allowing for the assessment of the impact of the hydrodynamic treatment duration on the macro and microparameters of porous structures.

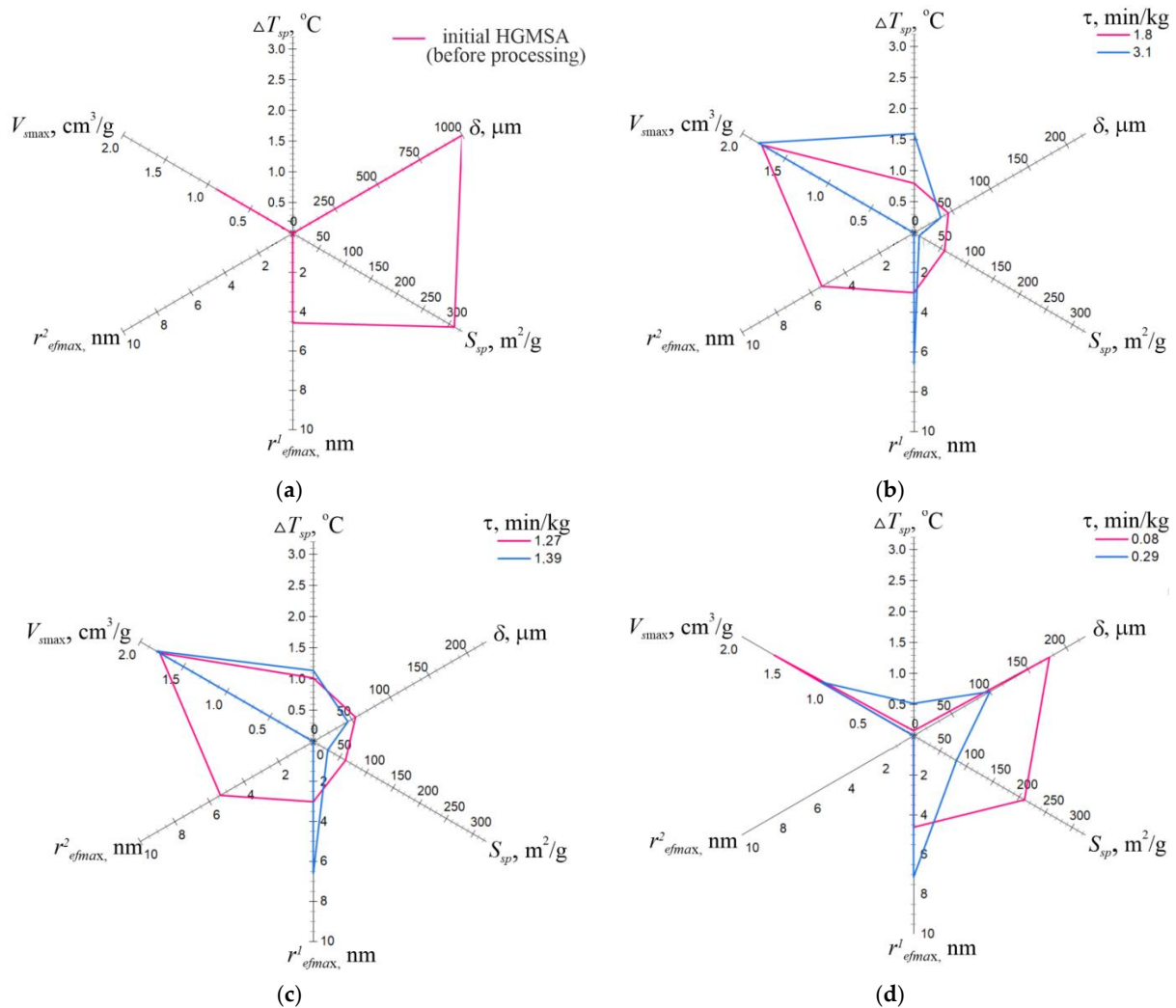


Figure 4. Histograms of the influence of hydrodynamic treatment on the structural and sorption characteristics of suspensions with HGMSA concentrations in H₂O: (a) 100% (initial HGMSA), (b) 70%, (c) 60%, (d) 40%; τ_{sp} —specific duration of processing; ΔT_{sp} —specific temperature increase; δ —is the average particle size; S_{sp} —specific surface area; r_{efmax}^1, r_{efmax}^2 —effective pore radius; V_s —the limiting sorption volume of pores.

For a non-concentrated suspension of “XGMSA-H₂O” with a hydrogel concentration of 40% (Figure 4d), a characteristic feature is the dissolution of an unstable framework originating from small monoliths, with the coagulation interaction predominating. The dispersion process of monoliths is concomitant with the alteration of their pore volume: initially, particles exhibit a broad range of fine pore sizes, but over time, fine pores undergo a ‘degeneration’ process, leading to the formation of monoliths with a more monoporous structure, accompanied by a reduction in the boundary sorption volume of pores.

With an increase in the hydrogel concentration in suspension to 60%, the nature of the histogram (Figure 4c) does not change, but the duration of the structure formation process is reduced. The influence of shear flow increases, leading to an increase in the dissipation of kinetic energy, which occurs due to the action of macroscopic viscous forces and the work of forces through the interfacial velocity nonequilibrium. By increasing the temperature during processing and changing its speed, it is possible to identify the transition of the suspension to a structured state.

The hydrogel concentration limit was set at 70%, at which the suspension has short-term fluidity properties in the recirculation circuit, which makes it possible to obtain a suspension with large sizes of monoliths with a highly developed S_{sp} surface and a

mesoporous structure (Figure 4b). In such a suspension, the contact (phase) interaction between particles at the macro and micro levels prevails.

3.2. Peculiarities of Xerogel Formation by Convective Drying Methods

Studies of hydrogel dehydration were carried out by two methods: convective drying in a layer and spraying in a heat carrier flow. The dehydration process was preceded by a hydrodynamic treatment stage until a fluid homogeneous suspension was obtained.

The results on experimental studies of the production of xerogels of methylsilicic acid xerogels (XGMSA) by convective drying in a layer with preliminary DPIE treatment of the initial suspension with a ratio of components of the HGMSA:H₂O system of 7:3 are shown in Table 2.

Table 2. Results of experimental studies of xerogel production by convective drying in a layer with preliminary DPIE treatment.

Sample #	DPIE Processing Parameters		Adsorption and Textural Characteristics of Xerogels						
	Number of Cycles	Temperature $T, ^\circ\text{C}$	Final Size of Monoliths in Suspension $\delta^H, \mu\text{m}$	Humidity $W, \%$	Specific Surface Area $S_{sp}, \text{m}^2/\text{g}$	Boundary Sorption Pore Volume $V_s, \text{cm}^3/\text{g}$	Effective Pore Radius $r_{ef\ max}, \text{nm}$	Pore Size Range d_{ef}, nm	Dimensions of Monoliths and Aggregates $\delta^X, \mu\text{m}$
1 (initial HGMSA)	-	-	up to 2×10^4	86	310	0.89	4.60	3–8	fragile loose-packed monoliths $1 \mu\text{m} \geq 2 \text{mm}$
2	1	19–20	60–290	91	210	1.62	4.61	3–28	monoliths 100–500 μm densely packed monoliths
3	10	19–28	30–156	91	32	0.45	2.81/8.89	2–40	>300 μm —85% 100–300 μm —7.6%

The highest specific surface area S_{sp} was observed for xerogels that were obtained from the original hydrogels without hydrodynamic treatment (sample #1). This sample consisted of xerogel monoliths with a brittle structure and a polydisperse composition (under slight mechanical loads, the monoliths are destroyed). On the basis of the composition and structure of the obtained sample, it can be concluded that the atomic type of contact interaction between particles predominates and the structure has a weak spatial framework.

A graphical interpretation of the data on the distribution of the sorption volume of pores by their size is shown in Figure 5.

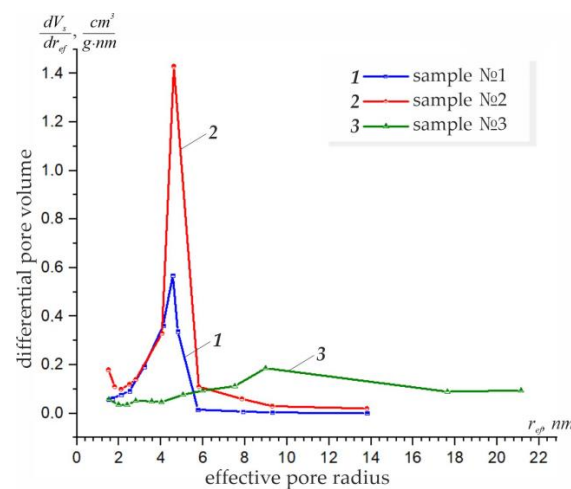


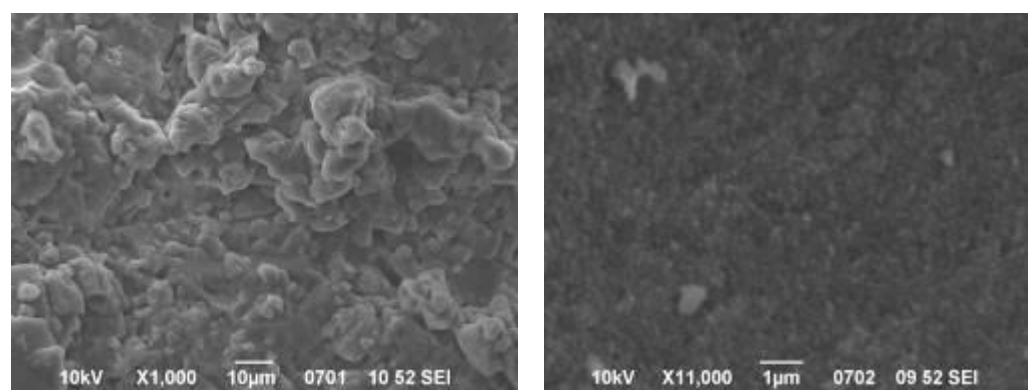
Figure 5. The size distribution of the volume of pores of xerogels obtained by convective drying in a layer: 1—a sample of the initial HGMSA; with preliminary hydrodynamic treatment: 2—sample processing #2 after 1 cycle; 3—sample #3 system after 10 cycles.

The results obtained indicate that sample #1 has a mesomodal monoporous structure with a rather narrow pore size range of 3–28 nm, which corresponds to the limit of the sorption pore volume $V_s = 0.89 \text{ cm}^3/\text{g}$. Furthermore, the pronounced maximum on the curve indicates the predominant pore size at the 9–10 nm level.

Studies have revealed that following one cycle of DPIE treatment, characterized by a specific treatment time of up to 0.1 min/kg, the dispersion of HGMSA in the liquid resulted in macro-level structural and textural transformations, while the porosity characteristics remained essentially unchanged. On the differential curve of sample #2 (2, Figure 5), a descending section is observed at the lower limit of the range of mesomodal pores, suggesting the presence of micropores in the structure. The treatment induced a decrease in the specific surface area (S_{sp}) by a factor of 1.5, while the pore volume (V_s) increased by nearly a factor of 2. Such transformations can be elucidated by structural changes, giving rise to new interparticle interactions with phase contacts, culminating in the formation of “secondary” pores.

Elevating the DPIE treatment duration to 10 recirculation cycles yields a more homogeneously dispersed suspension of hydrogel in water with reduced distribution values and particle sizes of HGMSA (sample #3). Upon the dehydration of such a suspension, robust monoliths were obtained, exhibiting an expanded range of pore sizes up to the upper limit of micropores and nearly reaching the lower limit of macropores (3, Figure 5). On the curve, distinctly pronounced maxima in the pore size intervals of 5 to 7 nm and 17 to 18 nm indicate size heterogeneity in the pore space. A comparison of the structural-textural characteristics of samples #3 and #2 reveals a substantial decrease in S_{sp} by 6.6 times and vs. by 3.6 times.

Morphological examinations of xerogels demonstrate that the original sample exhibits a uniform microrelief surface (Figure 6a), and one treatment cycle does not impact the surface topography with open surface pores (Figure 6b), elucidating the high structural-adsorption characteristics. Prolonged processing induces a shift in surface texture to a macrorelief (Figure 6c). The xerogels of the monoliths from sample #3 exhibit the highest structural and strength characteristics, owing to the compaction of the hydrogel structure with the degradation of micropores and partially of mesopores, resulting from the prolonged impact of landslide stresses during the passage through the rotary-pulsation apparatus.



(a)

Figure 6. Cont.

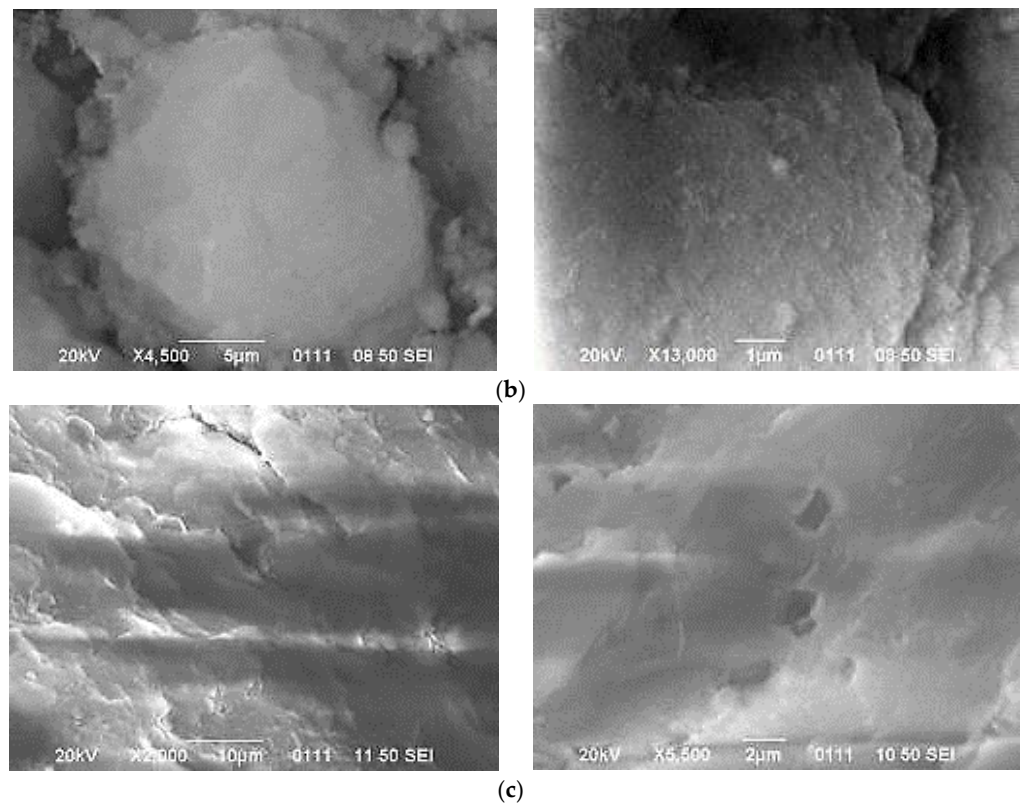


Figure 6. Surface morphology of xerogels after dispersion and drying in a layer of (a) initial HGMSA; (b) a suspension that has undergone one cycle of DPIE treatment; and (c) a system that has passed ten cycles of DPIE treatment.

The main parameters of the processes to obtain XGMSA by spray drying with a preliminary DPIE treatment of the HGMSA-H₂O suspension are given in Table 3.

Table 3. Process parameters for obtaining xerogels by spray drying with preliminary DIEI treatment.

Sample #	DPIE Process Parameters			Dewatering Process Parameters			
	Ratio of Suspension Components	Specific Time	Average Hydrogel Monoliths	Initial Humidity	Average Air Temperature in the Drying Chamber at the Inlet/Outlet	Final Humidity	Dispersion Characteristics of Xerogel Monoliths
		τ_{sp} , min/kg	δ^H , μm	W_p , %	$\frac{T_{in}}{T_{out}}$, °C	W_f , %	δ^X , μm
4	HGMSA:H ₂ O 7:3	2	60–290	93	206/87	0.5	<63–18%; 63–100–56%
5	Cu ²⁺ /Zn-HGMSA:H ₂ O 7:2	2	60–250	92		1.2	<5–80–14%; 15–30–80%

A comparative analysis of the morphology of two xerogel samples, featuring different ratios of components within the initial suspension (Figure 7) but obtained under identical process parameters, provides elucidation on the results of the variance analysis. Notable distinctions in the geometry and morphology of the monoliths are observed: sample #5, derived from a more concentrated suspension, exhibits a more uniform and highly dispersed composition, showcasing ellipsoidal monoliths, in contrast to sample #4. The latter is characterized by a polydisperse composition, displaying a broad range of monolith sizes and a less streamlined shape, while maintaining an open-pore microrelief on the surface. In the xerogel sample from the more concentrated suspension, the surface of the monolith nearly loses its microrelief.

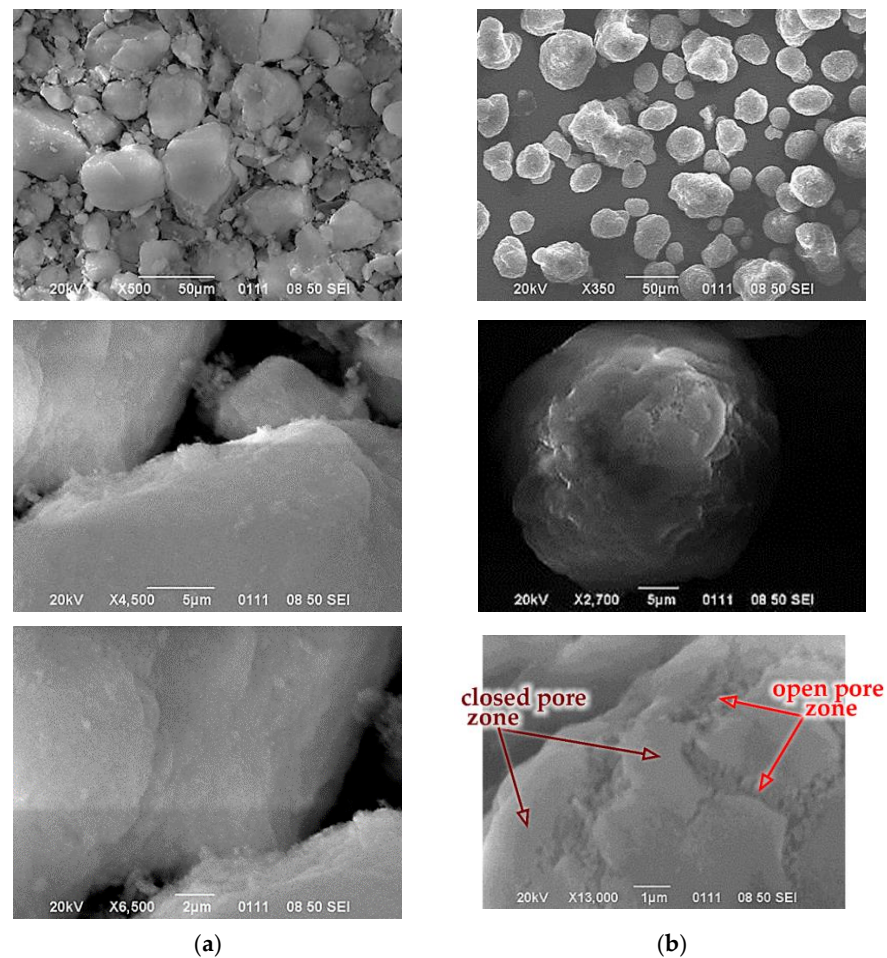


Figure 7. Morphology of xerogels obtained by spray drying with preliminary hydrodynamic treatment with hydrogel–H₂O ratio: (a) 7:3; (b) 7:2.

These results find explanation in the mechanism of suspension dehydration, which is inherently dependent on the structural and mechanical properties. A more concentrated suspension (sample #5) exhibits structural viscosity with a high yield strength, endowing hydrogel monoliths with a robust frame structure that withstands substantial shear deformations in the drying chamber. The brief exposure time suggests that closed pores are formed solely on the surface of the xerogel monolith, hindering the diffusion of moisture within the structure. Consequently, during dehydration, the surface layer experiences cracking, facilitating mass transfer through open pores. These production conditions result in elevated final moisture content in the xerogel powders, ranging from 1.2 to 1.5%, nearly three times higher than that observed for sample #4, characterized by a lower suspension yield strength. The shape of the monoliths and the polydisperse composition in this xerogel sample imply that monoliths with a loosely packed skeleton structure undergo disintegration during dehydration.

The xerogel monoliths obtained by sputtering have high structural-sorption parameters: $V_s = 1.6\text{--}1.8 \text{ cm}^3/\text{g}$, $S_{sp} = 280\text{--}291 \text{ m}^2/\text{g}$. The xerogel of sample #4 (Figure 8) has a structure with a wide range of mesopore sizes of 3–44 nm with a predominant size of 5–6 nm and 14–34 nm, while the xerogel of sample #5 has a polymodal set of pores 9–60 nm.

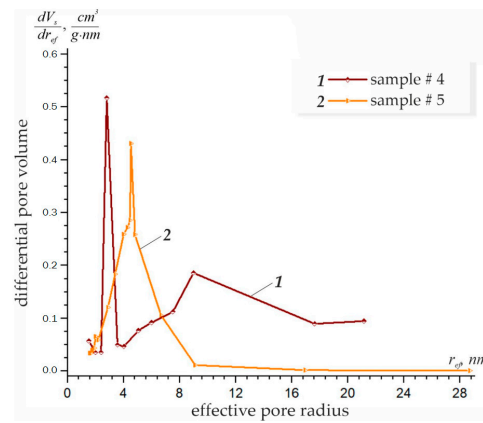


Figure 8. Distribution of sorption pore volume of xerogels by size, obtained by spray drying with preliminary hydrodynamic treatment with hydrogel–H₂O ratio: 1—7:3; 2—7:2.

This sample has a more monoporous structure with a maximum in the range of 26–30 nm, but with a lower limit sorption pore volume. It should be noted that macropores do not affect adsorption processes; however, they function as transport pores that ensure the diffusion of adsorbing substances to the surface of thin pores.

3.3. Rheological Behaviour of Hydrogel Suspensions

An analysis of the shear flows of concentrated suspensions (70% HGMSA in water) before and after liquid-phase dispersion (sample #2, Table 2) indicates the manifestation of complex rheological behavior, which is typical for structured disperse systems (Figure 9). The original suspension is polydisperse with loose aggregated particles $\delta^H = 500\text{--}2 \times 10^4 \mu\text{m}$, and the other is a more ordered structure with $\delta^H = 60\text{--}290 \mu\text{m}$.

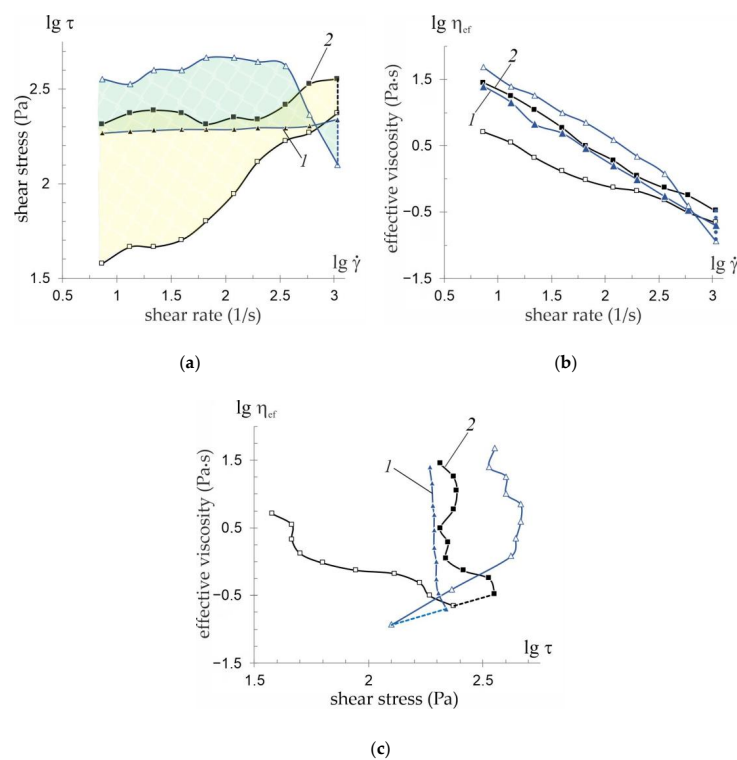


Figure 9. Full rheological curves of suspension HGMSA–H₂O in double logarithmic coordinates: (a) dependence of shear stress on shear rate; (b) dependence of effective viscosity on shear rate; (c) dependence of viscosity on shear stress: 1—initial suspension; 2—suspension after treatment. ▲ ■—load mode; △ □—unload mode; ● ●—hysteresis area of suspension flow before treatment and after hydrodynamic treatment.

The nature of the flow depends on the initial state of the dispersed system: the spread in the sizes of the hydrogel monoliths and their aggregates δ^H and the compactness of the aggregates. The destruction of aggregates of monoliths, the dimensions of which are greater than the critical δ_c^H , begins when $\dot{\gamma}$ reaches the value at which tensile hydrodynamic forces are able to break contact interactions between structured particles:

$$\delta_c^H \approx \frac{F_s^{0.5}}{\dot{\gamma}^{0.5}},$$

where F_s —is the adhesion force between the structural particles of the aggregate, normalized to its cross section.

The nonrotating flow curves in the so-called “loading”–“unloading” regimes, forming open hysteresis loops, signify the nonequilibrium state of the flow (Figure 9a). The mechanical stability of structured systems is quantified by the area enclosed within the hysteresis loop, and a decrease in this area denotes a restoration of mechanical stability to the system. The suspensions exhibit notable instability to shear deformations, with the initial suspension displaying greater mechanical stability, as indicated by its hysteresis loop area of $99.13 \times 10^3 \text{ Pa} \times \text{s}^{-1}$, compared to $135.14 \times 10^3 \text{ Pa} \times \text{s}^{-1}$ for the processed suspension.

Figure 9b,c reveal the absence of sections exhibiting a Newtonian flow trend, implying that the complete destruction of structural aggregates is not observed. As the shear rate increases, viscosity monotonically decreases over the studied range of $\dot{\gamma}$ by two orders of magnitude. While the curves for both suspensions in the ‘load mode’ exhibit similar behavior, the response of the suspensions to the removal of shear deformation differs significantly. This distinction can be attributed to the fact that, in the initial suspension, the shear deformation leads to a substantial reduction in the size of aggregates, resulting in an increased contact interaction surface. For such a system, the rate of the formation of new bonds between dispersed particles significantly surpasses the rate of the destruction of interaction between particles, unlike in a suspension that has undergone treatment.

In Figure 10, the dependency of viscosity change on the duration of the load at a fixed displacement rate is depicted. For the original system (1, Figure 10), the amplitude of fluctuations in viscosity values is lower than that observed for the processed system (2, Figure 10), indicating a tendency toward decreased fluctuations with an increasing duration of deformation. This suggests that the latter system exhibits a flow pattern closer to the equilibrium.

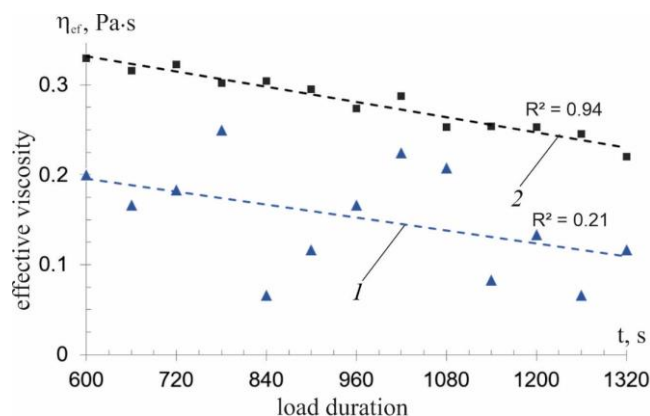


Figure 10. Dependence of the change in the viscosity of the “HGMSA-H₂O” suspension on time at $\dot{\gamma} = 1073 \text{ s}^{-1}$: 1—equilibrium curve for the initial system; 2—equilibrium curve of the suspension after treatment, \blacktriangle \blacksquare —experimental data.

For predictive estimates of the rheological behavior of pseudoplastic and viscous plastic systems, the various empirical models of Herschel–Buckley, Ostwald–de Wael, and

Casson [35,51,53] are taken into account, after which experimental data were approximated in the “load” mode in the range of shear rates 7–1080 s⁻¹.

The obtained dependence of the approximation with an estimate of the errors between the experimental and calculated values according to the models for the two studied structured systems are presented in Figure 11 and the parameters of the approximation models in Table 4.

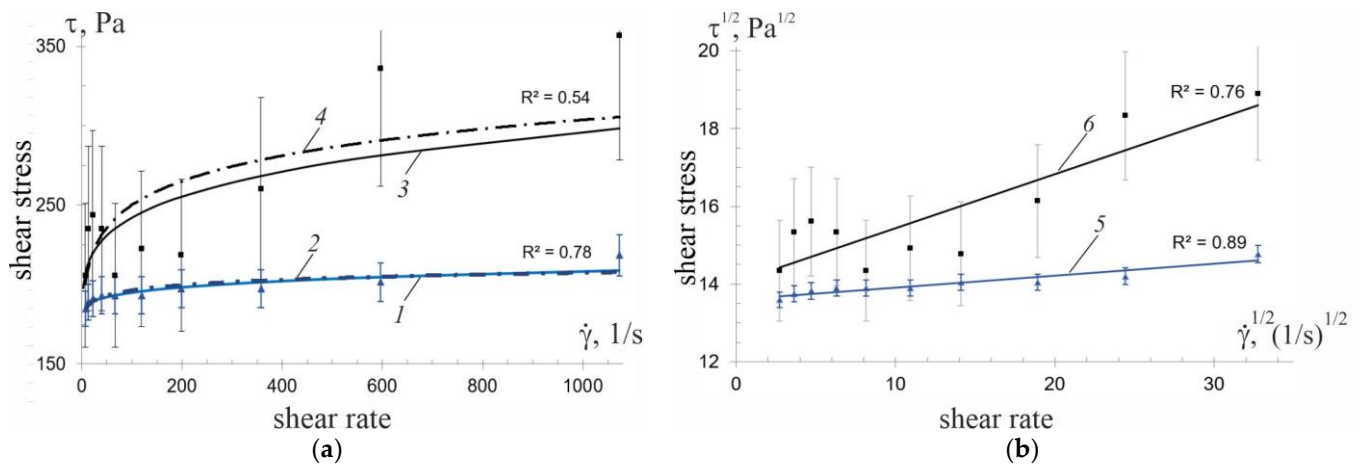


Figure 11. Flow approximation curves for the HGMSA-H₂O suspension: (a) Hershel-Buckley model and the Ostwald–de Waele model; (b) in coordinates according to the Casson model; 1, 3, 5—initial sample; 2, 4, 6—sample after processing.

Table 4. Rheological model approximation parameters *.

Suspension «HGMSA-H ₂ O»	Hershel-Buckley Model $\tau = \tau_0 + k\dot{\gamma}^n$				Ostwald–de Waele Model $\tau = k\dot{\gamma}^n$			Casson Model $\tau^{1/2} = \tau_0^{1/2} + (K\dot{\gamma})^{1/2}$		
	Equation Parameters			ε , %	Equation Parameters		ε , %	Equation Parameters		ε , %
	τ_0 , Pa	k	n		k	n		τ_0 , Pa	K , Pa·s	
initial	175.7	6.659	0.231	6	175.7	0.024	5	185.1	0.1×10^{-2}	2
after processing	169.6	23.92	0.241	22	169.6	0.084	20	197.23	0.019	8

* τ —dynamic shear stress; τ_0 —fluidity limit; $\dot{\gamma}$ —shear rate; k , K , n —rheological constants; ε —standard deviation.

For the initial suspension, according to the average approximation error ε at the level of 2–5%, the rheological models can be considered adequate. As for the treated suspension, the Casson model is closest to the experimental data. In the range of low shear rates, the relative error was 8%, and in the range of high and medium shear rates, 5%.

It should be noted that, for each of the shear-rate ranges, the nature of the flow of such structured suspensions has its own characteristics. Therefore, to improve the accuracy of predicting rheological behavior, an approximation is necessary for each of the shear-rate intervals. In addition, it should be taken into account that the region of low shear rates is especially sensitive.

An analysis of the suspensions deformation behavior of the studied under the action of a periodic load in the shear-rate range of 7–1073 s⁻¹ indicates a viscoplastic regime of their flow with a limiting shear stress of 170–205 Pa.

4. Conclusions

4.1. General Scientific Conclusions

The comprehensive research findings have established a foundation for the in-depth physical modeling of heat and mass transfer, as well as hydrodynamics, within the processing of organic–inorganic porous nanostructures produced through sol-gel technology.

Prolonging the duration of hydrodynamic treatment for hierarchical structures under shear deformations leads to a notable reduction in the boundary sorption volume of pores. This reduction is attributed to the disruption of monoporosity and the redistribution of pore space, involving the degradation of thin pores, the formation of new phase contacts, and the consequent emergence of “secondary” pores characterized by larger effective sizes towards macropores. Additionally, an increase in the concentration of hydrogel monoliths in suspensions accelerates macro-level structure-formation processes and influences the fluidity of suspensions within technological cycles.

The application of the microrheological Casson model is suggested for the anticipation of the rheological characteristics of dispersed systems with intricate structures, specifically in practical scenarios involving moderate shear rates within technological processes. The research outcomes elucidated the following objectives: investigating the flow patterns across low and high shear rates and facilitating the development of a generalized rheological model.

The results of a complex of scientific and technical studies made it possible to transfer technology for the manufacture of suspended forms of organosilicon enterosorbents; a plant was developed that passed industrial tests.

The acquired database serves as the foundational platform for advancing technologies in the production of pharmaceuticals and adsorption and catalytic materials for the purification of water and air from molecular pollutants. Additionally, it is instrumental in assessing their utility as fillers for energy-efficient coatings, with specific applications in window structures, in particular for the purpose of removing moisture from the air between window panes or as a heat insulator between panes.

4.2. Directions of Further Research and Their Preliminary Results

We are currently focused on the development of innovative technological processes for the creation of xerogels with antibacterial properties, specifically Methylsilicic Acid xerogels modified with copper ions (Cu^{2+} / Zn-XGMSA). An effective method for employing this xerogel involves air disinfection and purification through inactivating aerosolized streams of airborne pathogens, including the SARS-CoV-2 virus, and neutralizing molecular pollutants via ozone technologies based on plasma chemical methods. To ensure the safe utilization of ozone technologies, we employ excess ozone destruction using adsorption-catalytic filters founded on porous xerogel matrices. Ongoing tests on an experimental setup with flow-circulating plasma-chemical air treatment reactors aim to examine the decontamination kinetics of sanitary-indicative microorganisms under diverse aerodynamic conditions.

This scientific direction aligns closely with the imperative of sustainable human development, particularly in light of the profound repercussions of the pandemic, which resulted in significant human tolls, with 765 million individuals contracting COVID-19 and 6.9 million fatalities [54], alongside a notable decline of 3.4% in the global GDP in 2020 [55]. It is envisaged that our findings pertaining to the purification and disinfection of ventilation air within buildings will offer a meaningful contribution towards mitigating the potential risks associated with epidemiological infections among the populace.

Our research into the thermal conductivity of aerogels underscores their efficacy as thermal insulators. Specifically, the coefficients of thermal conductivity observed for powdered xerogels MSA, with a moisture content (W) of 0.5%, densities ranging from 200 to 350 kg/m^3 , and particle sizes spanning from 20 to 120 μm , fall within the range of 0.034–0.037 $\text{W}/(\text{m}\cdot^\circ\text{C})$. Notably, XGMSA exhibits even lower values, ranging from 0.023 to 0.028 $\text{W}/(\text{m}\cdot^\circ\text{C})$, surpassing those of air. Furthermore, aerogels demonstrate even lower coefficients of thermal conductivity, rendering them suitable for insulating building facades

and industrial equipment. Preliminary investigations into the incorporation of powdered xerogels into paints and varnishes have yielded promising results, showing enhanced heat resistance and reduced heat loss to the environment.

Preliminary experiments involving plates constructed from nanostructured aerogels, supplemented with low-emission coatings, corroborate their potential to significantly enhance the energy efficiency of cutting-edge window structures [56]. Concurrently, this approach leads to notable reductions in heat dissipation from buildings to the environment, thereby offering a tangible contribution towards mitigating global warming stemming from the energy sector [57]. This aligns directly with the principles of sustainable development.

4.3. Financial Support

This article was supported by the Ukrainian National Research Foundation under Project No. 2022.01/0172, focusing on “Aerodynamics, Heat Transfer, and Innovations to Enhance Energy Efficiency of Window Structures for Restoring War-Damaged Buildings in Ukraine”.

Author Contributions: Conceptualization, B.B. and T.H.; methodology, H.K.; formal analysis, B.B.; investigation, A.P.; resources, H.K.; data curation, T.H. and H.K.; writing—original draft preparation, A.P.; writing—review and editing, T.H. and H.K.; visualization, T.H.; supervision, A.P. and V.O.; project administration, V.O.; funding acquisition, B.B. All authors have read and agreed to the published version of the manuscript.

Funding: This article was supported by the Ukrainian National Research Foundation under Project No. 2022.01/0172, focusing on “Aerodynamics, Heat Transfer, and Innovations to Enhance Energy Efficiency of Window Structures for Restoring War-Damaged Buildings in Ukraine”.

Institutional Review Board Statement: Not applicable.

Informed Consent Statement: Not applicable.

Data Availability Statement: Data are contained within the article.

Conflicts of Interest: The authors have no competing interests that might be perceived to influence the results and discussion reported in this paper.

References

1. Akhtar, F.; Andersson, L.; Ogunwumi, S.; Hedin, N.; Bergström, L. Structuring adsorbents and catalysts by processing of porous powders. *J. Eur. Ceram. Soc.* **2014**, *34*, 1643–1666. [[CrossRef](#)]
2. Basok, B.; Davydenko, B.; Koshlak, H.; Novikov, V. Free Convection and Heat Transfer in Porous Ground Massif during Ground Heat Exchanger Operation. *Materials* **2022**, *15*, 4843. [[CrossRef](#)]
3. Lobanov, L.M.; Chalaev, D.M.; Goncharov, P.V.; Grabova, T.L.; Pashchin, M.O.; Goncharova, O.M.; Sydorenko, V.V. Development of Equipment for Air Decontamination in the Ventilation and Air Conditioning Systems of Public Buildings with the Use of the Photocatalysis and Plasmachemistry Methods. *Sci. Innov.* **2023**, *19*, 57–71. [[CrossRef](#)]
4. Mazzotta, E.; De Santo, M.; Lombardo, D.; Leggio, A.; Pasqua, L. Mesoporous silicas in materials engineering: Nanodevices for bionanotechnologies. *Mater. Today Bio* **2022**, *17*, 100472. [[CrossRef](#)]
5. Gomez, G.E.; Hamer, M.; Regiart, M.D.; Tortella, G.R.; Seabra, A.B.; Soler Illia, G.J.A.A.; Fernández-Baldo, M.A. Advances in Nanomaterials and Composites Based on Mesoporous Materials as Antimicrobial Agents: Relevant Applications in Human Health. *Antibiotics* **2024**, *13*, 173. [[CrossRef](#)] [[PubMed](#)]
6. Grisolia, A.; Dell’Olio, G.; Spadafora, A.; De Santo, M.; Morelli, C.; Leggio, A.; Pasqua, L. Hybrid Polymer-Silica Nanostructured Materials for Environmental Remediation. *Molecules* **2023**, *28*, 5105. [[CrossRef](#)] [[PubMed](#)]
7. Jambhrunkar, M.; Maghrebi, S.; Doddakyanahalli, D.; Wignall, A.; Prestidge, C.A.; Bremmell, K.E. Mesoporous Organosilica Nanoparticles to Fight Intracellular Staphylococcal Aureus Infections in Macrophages. *Pharmaceutics* **2023**, *15*, 1037. [[CrossRef](#)] [[PubMed](#)]
8. Vallet-Regí, M.; Schüth, F.; Lozano, D.; Colilla, M.; Manzano, M. Engineering mesoporous silica nanoparticles for drug delivery: Where are we after two decades? *Chem. Soc. Rev.* **2022**, *51*, 5365–5451. [[CrossRef](#)]
9. Yu, A.; Dai, X.; Wang, Z.; Chen, H.; Guo, B.; Huang, L. Recent Advances of Mesoporous Silica as a Platform for Cancer Immunotherapy. *Biosensors* **2022**, *12*, 109. [[CrossRef](#)]
10. Zhou, Z.; Wu, W.; Fang, J.; Yin, J. Polymer-based porous microcarriers as cell delivery systems for applications in bone and cartilage tissue engineering. *Int. Mater. Rev.* **2021**, *66*, 77–113. [[CrossRef](#)]

11. El-Samak, A.A.; Ponnammam, D.; Hassan, M.K.; Ammar, A.; Adham, S.; Al-Maadeed, M.A.A.; Karim, A. Designing flexible and porous fibrous membranes for oil water separation—A review of recent developments. *Polym. Rev.* **2020**, *60*, 671–716. [[CrossRef](#)]
12. Ye, S.; Wang, B.; Shi, Y.; Wang, B.; Zhang, Y.; Feng, Y.; Han, W.; Liu, C.; Shen, C. Superhydrophobic and superelastic thermoplastic polyurethane/multiwalled carbon nanotubes porous monolith for durable oil/water separation. *Compos. Commun.* **2020**, *21*, 100378. [[CrossRef](#)]
13. Kovylin, R.S.; Yudin, V.V.; Shurygina, M.P.; Fedoseev, V.B.; Chesnokov, S.A.; Fedushkin, I.L.; Piskunov, A.V. Porogen Concentration Effect on the Pore Structure and Properties Evolution of Polymer Monolith Based on Oligocarbonate Dimethacrylate OCM-2. *Materials* **2023**, *16*, 3177. [[CrossRef](#)]
14. Haider, Z.; Haleem, A.; Farooq, U.; Shi, L.; Claver, U.P.; Memon, K.; Memon, K.; Fareed, A.; Khan, I.; Mbogba, M.K.; et al. Highly porous polymer cryogel based tribopositive material for high performance triboelectric nanogenerators. *Nano Energy* **2020**, *68*, 104294. [[CrossRef](#)]
15. Irzhak, V.I. Percolation Threshold in Polymer Nanocomposites. *Colloid J.* **2021**, *83*, 64–69. [[CrossRef](#)]
16. Ni, X.; Hui, C.; Su, N.; Cutler, R.; Liu, F. A 3D percolation model for multicomponent nanocarbon composites: The critical role of nematic transition. *Nanotechnology* **2019**, *30*, 185302. [[CrossRef](#)]
17. Gregg, S.J.; Sing, K.S.W. *Adsorption, Surface Area and Porosity*, 2nd ed.; Academic Press: London, UK, 1982; ISBN 0-12-300956-1. [[CrossRef](#)]
18. Ahmad, A.; Khan, S.; Tariq, S.; Luque, R.; Verpoort, F. Self-sacrifice MOFs for heterogeneous catalysis: Synthesis mechanisms and future perspectives. *Mater. Today* **2022**, *55*, 137–169. [[CrossRef](#)]
19. Aijaz, M.O.; Yang, S.B.; Karim, M.R.; Alnaser, I.A.; Alahmari, A.D.; Almubaddel, F.S.; Assaifan, A.K. Preparation and Characterization of Electrospun Poly(lactic acid)/Poly(ethylene glycol)-b-poly(propylene glycol)-b-poly(ethylene glycol)/Silicon Dioxide Nanofibrous Adsorbents for Selective Copper (II) Ions Removal from Wastewater. *Membranes* **2023**, *13*, 54. [[CrossRef](#)] [[PubMed](#)]
20. Koshlak, H. Synthesis of zeolites from coal fly ash using alkaline fusion and its applications in removing heavy metals. *Materials* **2023**, *16*, 4837. [[CrossRef](#)]
21. Groult, S.; Buwalda, S.; Budtova, T. Pectin hydrogels, aerogels, cryogels and xerogels: Influence of drying on structural and release properties. *Eur. Polym. J.* **2021**, *149*, 110386. [[CrossRef](#)]
22. Homburg, S.V.; Patel, A.V. Silica Hydrogels as Entrapment Material for Microalgae. *Polymers* **2022**, *14*, 1391. [[CrossRef](#)]
23. Al Soubaihi, R.M.; Saoud, K.M.; Ye, F.; Myint MT, Z.; Saeed, S.; Dutta, J. Synthesis of hierarchically porous silica aerogel supported Palladium catalyst for low-temperature CO oxidation under ignition/extinction conditions. *Microporous Mesoporous Mater.* **2020**, *292*, 109758. [[CrossRef](#)]
24. McNaught, A.D.; Wilkinson, A. (Eds.) *IUPAC Compendium of Chemical Terminology*; Gold Book, Version 2.3.3; International Union of Pure and Applied Chemistry: Research Triangle Park, NC, USA, 2014. [[CrossRef](#)]
25. Guizard, C.G.; Julbe, A.; Ayrat, A. Design of nanosized structures in sol-gel derived porous solids. Applications in catalyst and inorganic membrane preparation. *J. Mater. Chem.* **1999**, *9*, 55–65. [[CrossRef](#)]
26. Budnyak, T.M.; Yanovska, E.S.; Kołodyn'ska, D.; Sternik, D.; Pylypchuk, I.V.; Ischenko, M.V.; Tertyk, A.V. Preparation and properties of organomineral adsorbent obtained by sol-gel technology. *J. Therm. Anal. Calorim.* **2016**, *125*. [[CrossRef](#)]
27. Turchina, T.; Zhukotsky, E.; Dekusha, G.; Makarenko, A. Influence of structuring additive on output mushrooms powder when drying by spraying method. *Sci. Work.* **2020**, *84*, 67–75. [[CrossRef](#)]
28. Nandiyanto, A.B.D.; Ogi, T.; Wang, W.-N.; Gradon, L.; Okuyama, K. Template-assisted spray-drying method for the fabrication of porous particles with tunable structures. *Adv. Powder Technol.* **2019**, *30*, 2908–2924. [[CrossRef](#)]
29. Pavlenko, A.M.; Basok, B.I. Kinetics of water evaporation from emulsions. *Heat Transf. Res.* **2005**, *36*, 425–430. [[CrossRef](#)]
30. Basok, B.I.; Davydenko, B.V.; Avramenko, A.O.; Pirozhenko, I.O. *Hydrodynamics, Heat Transfer and Crushing Effects in Rotationally Pulsating Flows*; Monograph; Express: Kyiv, Ukraine, 2012; 298p, ISBN 978-966-02-6716-9. Available online: https://www.studmed.ru/basok-b-i-davydenko-b-v-avramenko-a-a-pirozhenko-i-a-gidroinamika-teploobmen-i-effekty-drobleniya-vo-vraschatelno-pulsiruyuschih-potokah-rotorno-pulsacionnyy-apparat-rpa_0ce44dd1f0f.html (accessed on 18 January 2024).
31. Uriev, N.B. *Technology of Dispersed Systems and Materials: Physicochemical Dynamics of Structure Formation and Rheology*; Monograph; Wiley-VCH Verlag GmbH & Co. KGaA: Weinheim, Germany, 2017; ISBN 978-3-527-80619-5.
32. Dolinsky, A.A.; Avramenko, A.A.; Tyrinov, A.I.; Grabova, T.L. Study of the Dynamics of formation of Spatial Nanostructures. In *Nanoplasmonics, Nano-Optics, Nanocomposites and Surface Studies: Springer Proceedings in Physics*; Fesenko, O., Yatsenko, L., Eds.; Springer International Publishing: Cham, Switzerland, 2015; Volume 167, pp. 223–232. [[CrossRef](#)]
33. Pavlenko, A.; Koshlak, H.; Basok, B. Application of thermal and cavitation effects for heat and mass transfer process intensification in multicomponent liquid media. In Proceedings of the 7th Thermal and fluids Engineering Conference (TfEC-2022), Las Vegas, NV, USA, 16–18 May 2022; pp. 1267–1284. [[CrossRef](#)]
34. Delaplace, G.; Gu, Y.; Liu, M.; Jeantet, R.; Xiao, J.; Chen, X.D. Homogenization of liquids inside a new soft elastic reactor: Revealing mixing behavior through dimensional analysis. *Chem. Eng. Sci.* **2018**, *192*, 1071–1080. [[CrossRef](#)]
35. Fatimi, A.; Tassin, J.F.; Bosco, J.; Deterre, R.; Axelos, M.A.; Weiss, P. Injection of calcium phosphate pastes: Prediction of injection force and comparison with experiments. *J. Mater. Sci. Mater. Med.* **2012**, *23*, 1593–1603. [[CrossRef](#)]
36. Both, E.M. Powder Morphology Development during Spray Drying. Ph.D. Thesis, Wageningen University, Wageningen, The Netherlands, 2019; 130p. [[CrossRef](#)]

37. Siemons, I.; Vaessen EM, J.; Van Peski, S.O.; Boom, R.M.; Schutyser, M.A.I. Protective effect of carrier matrices on survival of *Lactobacillus plantarum* WCFS1 during single droplet drying explained by particle morphology development. *J. Food Eng.* **2021**, *292*, 110263. [CrossRef]
38. Slinyakova, I.B.; Denisova, T.I. *Silicone Adsorbents: Preparation, Properties, Application*; Monograph; Naukova Dumka: Kyiv, Ukraine, 1988; 190p, ISBN 5-12-000224-2.
39. Wu, T.; Ke, Q.; Lu, M.; Pan, P.; Zhou, Y.; Gu, Z.; Cui, G.; Lu, H. Recent Advances in Carbon-Silica Composites: Preparation, Properties, and Applications. *Catalysts* **2022**, *12*, 573. [CrossRef]
40. Kraiwattanawong, K.; Sano, N.; Tamon, H. Influence of Evaporation Drying on the Porous Properties of Carbon/Carbon Composite Xerogels. *Polymers* **2021**, *13*, 2631. [CrossRef]
41. Kohns, R.; Torres-Rodríguez, J.; Euchler, D.; Seyffertitz, M.; Paris, O.; Reichenauer, G.; Enke, D.; Huesing, N. Drying of Hierarchically Organized Porous Silica Monoliths—Comparison of Evaporative and Supercritical Drying. *Gels* **2023**, *9*, 71. [CrossRef]
42. Yashina, N.I.; Plygan, E.P.; Semenov, V.G. Sol-Gel Technology of the Mesoporous Methylsilicic Acid Hydrogel: Medicine Aspects of Globular Porous Organosilicon Materials Application. In *Sol-Gel Methods for Material Processing*; NATO Science for Peace and Security Series C: Environmental Security; Springer: Dordrecht, The Netherlands, 2008; pp. 481–488. [CrossRef]
43. Enterosgel Research. *Innovative Enterosorption Method*; EnteroMed Limited: London, UK, 2015. Available online: <https://enterosgel.it/upload/iblock/275/2750602317e6d4d475016895976e7aae.pdf> (accessed on 5 January 2024).
44. Shevchenko, Y.; Dushanin, B.; Polianskyi, O.; Yashina, N. Methyl-Silicic Acid Hydrogels as Adsorbing Agents of Middle Molecular Weight Metabolites and Process for the Preparation Thereof. UA Patent 7472A, 26 February 1999. Available online: <https://uapatents.com/7-7472-gidrogeli-metil kremniehvo-kisloti-enterosgel-super-yak-adsorbenti-seredno-molekulyarnikh-metabolitiv-ta-sposib-kh-oderzhannya.html> (accessed on 10 June 2023).
45. Tolcheyev, Y.; Chygyryk, O.; Semenov, V. Method for Producing Asorbent Based on a Methyl-Silicic Acid Hydrogel. U.S. Patent 2010/0240532 A1, 23 September 2010. Available online: <https://patentimages.storage.googleapis.com/88/e7/35/58538c52ebb7be/US20100240532A1.pdf> (accessed on 10 June 2023).
46. Obodovich, O.; Grabova, T.; Posunko, D.; Bazieiev, R. Implementation of the DPIE method in technologies of obtaining structured systems. *Thermophys. Therm. Power Eng.* **2021**, *43*, 13–20. [CrossRef]
47. Hrabov, L.M.; Merschii, V.I.; Zhylieiev, V.T. Reactron Homogenizer. UA Patent 20698, 15 April 2002. Available online: <https://sis.nipo.gov.ua/uk/search/detail/326568/> (accessed on 5 January 2024).
48. Dolinsky, A.; Grabova, T.; Stepanova, O. Creation and introduction the effective technologies and equipment for the manufacture of pharmaceuticals. Part 1. *Thermophys. Therm. Power Eng.* **2017**, *37*, 31–43. [CrossRef]
49. Dolinsky, A.A.; Avramenko, A.O.; Ivanytskyi, G.K. Use of DPIE Mechanisms and Methods to Control the Kinetics of Nanolevel Processes. *Visnyk Natl. Acad. Sci. Ukr.* **2013**, *8*, 47–57. Available online: <http://dspace.nbuv.gov.ua/handle/123456789/67871> (accessed on 21 May 2023).
50. Pavlenko, A.M.; Basok, B.I.; Avramenko, A.A. Heat conduction of a multi-layer disperse particle of emulsion. *Heat Transf. Res.* **2005**, *36*, 55–61. [CrossRef]
51. Dro´zdzziel, P.; Vitenko, T.; Voroshchuk, V.; Narizhnyy, S.; Snizhko, O. Discrete-Impulse Energy Supply in Milk and Dairy Product Processing. *Materials* **2021**, *14*, 4181. [CrossRef]
52. Dolinsky, A.; Maletska, K. Spray drying. In *Heat Technologies and Equipment for Obtaining Powder Materials*; Monograph; Akademi-periodika: Kyiv, Ukraine, 2015; Volume 2, 390p, ISBN 978-966-360-300-1.
53. Jankowska, H.; Dzido, A.; Krawczyk, P. Determination of Rheological Parameters of Non-Newtonian Fluids on an Example of Biogas Plant Substrates. *Energies* **2023**, *16*, 1128. [CrossRef]
54. Number of Novel Coronavirus (COVID-19) Confirmed Cases and Deaths as of April 26, 2023, by Region. Available online: <https://www.statista.com/topics/6139/covid-19-impact-on-the-global-economy/#editorsPicks> (accessed on 5 January 2024).
55. Impact of the Coronavirus Pandemic on the Global Economy—Statistics & Facts. Available online: <https://www.statista.com/topics/6139/covid-19-impact-on-the-global-economy/#topicOverview> (accessed on 5 January 2024).
56. Koshlak, H.; Basok, B.; Davydenko, B. Heat Transfer through Double-Chamber Glass Unit with Low-Emission Coating. *Energies* **2024**, *17*, 1100. [CrossRef]
57. Basok, B.I.; Bazeev, Y.T.; Dubovsky, S.V. *Energy and Global Warming*; Scientific Thought: Kyiv, Ukraine, 2023; 172p, ISBN 978-966-00-1841-9. [CrossRef]

Disclaimer/Publisher’s Note: The statements, opinions and data contained in all publications are solely those of the individual author(s) and contributor(s) and not of MDPI and/or the editor(s). MDPI and/or the editor(s) disclaim responsibility for any injury to people or property resulting from any ideas, methods, instructions or products referred to in the content.